

# Unique Current Conduction Mechanism through Multi Wall CNT Interconnects under ESD Conditions

Abhishek Mishra and Mayank Shrivastava

Advanced Nanoelectronic Device & Circuit Research Group, Department of Electronic Systems Engineering  
Indian Institute of Science, Bangalore, 560012, India, email: mayank@dese.iisc.ernet.in

**Abstract** - We present unique physics of ESD current transport through Multi-wall Carbon Nanotubes. Role of substrate, CNT shells and sub-bands in ESD current conduction is highlighted. The quantum electron-phonon transport under non-equilibrium (ESD) conditions is explained using CNT band structure and interplay between electrical and thermal transport along the nanotube.

## I. Introduction

Multi-wall Carbon Nanotubes (MWCNTs) are possible replacements of conventional copper-based interconnects [1,2]. Their benefits include high current carrying capacity, resistance to electromigration, high thermal conductivity and high strength due to strong  $sp^2$  bonds between carbon atoms. This emerging material has attracted promising inputs and developments from almost all corners of the fraternity. Compact models [3], various reliability theories [4] and fabrication processes [5] are already available. ESD analysis of these tubes was recently studied in [6] – [8], where the unique shell-by-shell failure of these tubes was highlighted. In the present work, we perform a comprehensive experimental investigation and theoretical analysis of ESD current conduction through these nanotubes.

## II. Device Fabrication

Tubes used in this work were grown by thermal CVD, and thick tubes (50 nm in diameter) with current-carrying capacity of more than  $50 \mu\text{A}$  were selected for ESD measurements. Post growth, tubes were dielectrophoretically deposited across metal electrodes [9]. A stack of chrome-palladium was deposited on  $\text{SiO}_2$ , pre-patterned using electron-beam lithography. After deposition, devices were properly cleaned with acetone/IPA, followed by dehydration bake at  $250^\circ\text{C}$  to remove any organic contamination. This deposition technique was selected as it results in side-contacted tubes. Such a contact is best suited for studying current conduction mechanism through individual shells as only the outermost shell is electrically connected to the metal contact. Two different configurations of side-contacted tubes were selected for TLP measurements – (1) short suspended tubes (2) long substrate-supported tubes. The former configuration does not contact the substrate, while a

major fraction of the length of latter configuration rests on the substrate. ESD investigations were performed using a TLP setup with ultra-low current ( $\sim 50 \mu\text{A}$ ) sensing capability (figure 1c). Low current was sensed by using - 1) current sensor with sensitivity of  $5 \text{ mV}/\text{mA}$ ; 2) mixed-domain oscilloscope with resolution of  $1 \text{ mV}/\text{div}$ . The TLP system was well calibrated against a standard SMD resistor and Zener diode. The current sensor shows low-frequency roll-off for pulse-widths of more than  $6.3 \mu\text{s}$  ( $L/R$  time constant). Measurements reported in the work were done for pulse-widths  $\leq 100 \text{ ns}$ , therefore the low-frequency effects (droop) can be safely neglected.

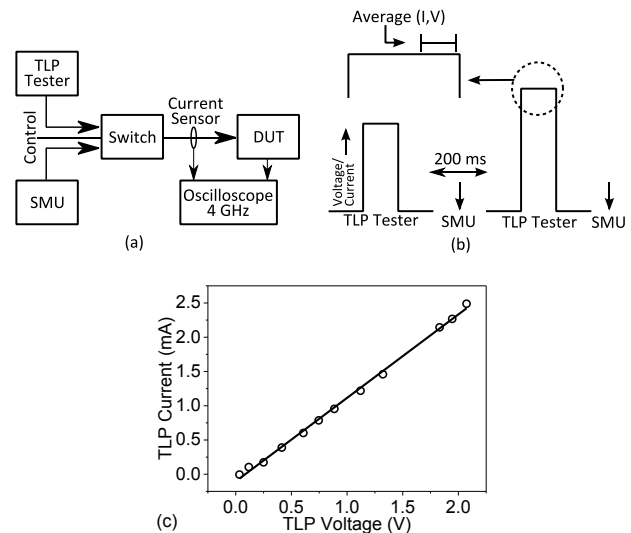


Figure 1: (a) Experimental setup for emulating ESD stress through MWCNTs. All cables and ports are  $50 \Omega$  matched. (b) Analysis technique: Low bias ( $500 \text{ mV}$ ) DC current is extracted after each pulse, while the response towards pulsed voltage is averaged in a window from 70% to 90% of the pulse width. (c) TLP characteristic of an SMD resistor. The curve shows linear behavior in both sub-mA and mA range.

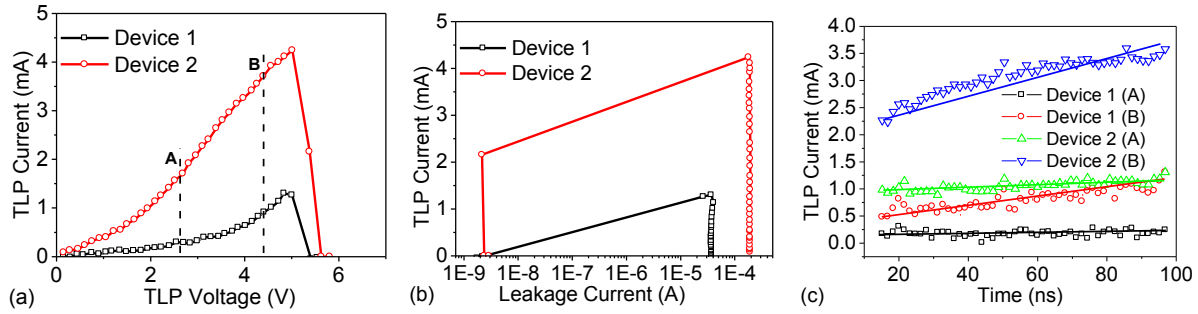


Figure 2: (a) TLP characteristics of suspended tubes (b) change in low-bias leakage with TLP current (c) Transient waveforms at two different TLP voltages marked in (a). Note that current remains constant with time at bias point marked *A*, while at point *B*, it increases linearly with time.

Unless stated otherwise, pulse width of 100 ns and rise time of 1 ns was used for all the measurements. To study failure, low-bias device resistance was closely monitored after every ESD stress pulse (figure 1). Since the interconnects based on MWCNTs are still in budding stage and need more improvements at process and modeling fronts, therefore, instead of reporting current per unit footprint, raw TLP current is reported. Nevertheless, the TLP current can be converted to current per unit footprint by using footprint area of  $L \times d$ , where  $L$  and  $d$  denotes length and diameter of the tube respectively.

### III. Conduction through Suspended MWCNTs

Figure 2 shows TLP characteristics of suspended MWCNTs (figure 4) and highlights the following key features – (1) rise in TLP current shifts from linear to exponential after a particular threshold voltage (figure 2a), (2) current w.r.t. time remains unchanged during the linear branch of the TLP current-voltage characteristics, while it increases linearly with time for currents in the exponential branch of the TLP current-voltage characteristics (figure 2c). In order to explain the unique behavior under ESD conditions, Landauer's formulation [10] for electrical conduction through individual shells of MWCNT is referred.

$$I = \frac{2e}{h} M \bar{T} (\mu_1 - \mu_2) \quad (1)$$

where,  $\mu_1 - \mu_2 =$  TLP voltage,  $\bar{T}$  is the transmission coefficient through the nanotube and  $M$  is the number of conduction channels. Unlike bulk materials, the circumferential quantization in these materials results in a series of sub-bands. The sum of these sub-bands, weighted with Fermi-Dirac function defines the number of conduction channels available for conduction. Analytically, for a thick shell with diameter  $D$ , the number of channels participating in conduction at temperature  $T$  is given by [3]:

$$M(D, T) = aTD + b \quad (2)$$

where,  $a$  and  $b$  are constants, whose values depends on thermal energy of electrons and gap between sub-bands. Consequently, number of conduction channels and hence electrical current (eq. 1) through the tube depends linearly on temperature. Under high ESD stress conditions, hot contact of suspended tube becomes a reservoir of phonons, while the cold contact acts as a sink for phonons. The difference in phonon population drives heat flux from hot to cold contact, along length of the tube (figure 3).

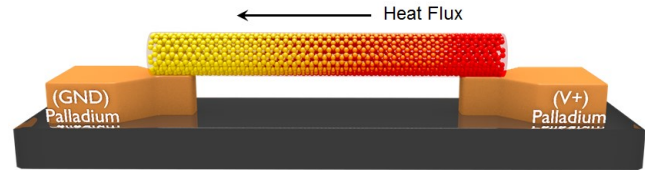


Figure 3: Heat transport from hot contact (V+) to cold contact (GND). The propagation starts at  $t = 0^+$  and continues till a state of thermal equilibrium is reached. Hot and cold refers to energy of carriers at the respective electrodes.

The consequent heating-up of cold contact results in linear increase in number of conduction channels and current, as predicted by equations 1 and 2. This process continues during the entire state of thermal non-equilibrium.

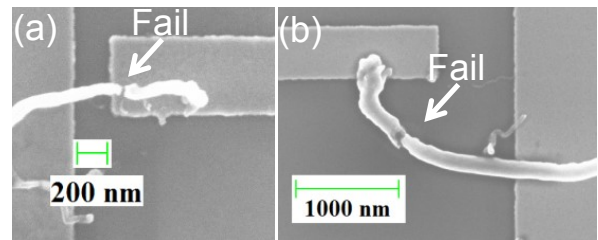


Figure 4: (a) SEM image of (a) Device 1 & (b) Device 2 after shell by shell failure. Both the devices are suspended between metal electrodes. Note that the devices have failed near contact, indicating ballistic transport through the tube.

The other key feature of the TLP characteristics shown in figure 2(a) is the exponential rise in current with voltage. Conduction through individual shells of a CNT happens via band-to-band tunneling of

electrons from valence band to conduction band (figure 5). The two requirements of tunneling are (1) band-bending enough to cause sufficiently high probability of tunneling, (2) empty states in conduction band and filled states in valence band. The former condition requires a threshold voltage above which current rises exponentially, while requirement of the latter condition is fulfilled by thermal-assisted rise in number of conduction channels as explained earlier. The overall conduction mechanism follows thermal assisted band-to-band tunneling, a mechanism unique to multi-wall carbon nanotubes (figure 5).

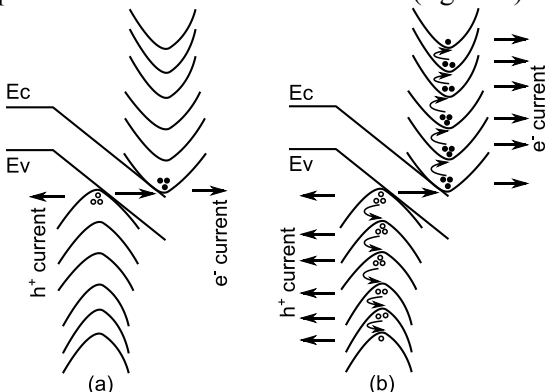


Figure 5: Occupancy of sub-bands at (a)  $t = 0^+$  and (b)  $t \geq t_{\text{equilibrium}}$ . Band diagrams are shown for interface at the cold contact.

At  $t = 0^+$ , depending on temperature and diameter,  $S_1$  number of sub-bands participate in conduction. Conduction at this instant happens primarily due to direct transmission through crossing sub-bands and tunneling through nearest available sub-bands [11]. As explained earlier, temperature of the cold contact keeps increasing due to flux of heat from hot to cold contact. Increase in temperature smears-up the Fermi-Dirac distribution of electrons, and increases the number of sub-bands to  $S_2 (>S_1)$ . Consequently, more states become available for tunneling, which eventually results in exponential rise in current. This process continues till  $t = t_{\text{equilibrium}}$ , at which the device attains thermal equilibrium and stops any further increase in participation of sub-bands.

In the discussion presented so far, it is assumed that the transport through the tube is ballistic in nature. Analysis of SEM images in figure 4 justifies the validity of this assumption. Channel of ballistic tube remains devoid of scattering, and most of the collisions happen at the hot contact and nanotube interface, due to which ballistic tube breaks near the contact. Tubes in figure 4 show damage near the contact, which proves the ballistic nature of the tubes.

#### IV. Conduction through Substrate-Supported MWCNTs

Substrate plays a crucial role in deciding thermal and electrical transport through MWCNTs. Underlying substrate not only increases scattering, but also provides a medium for heat dissipation from MWCNT to the substrate. Hence, it is imperative to study the effect of substrate on conduction of ESD current. Figure 6 shows TLP characteristics of substrate-supported MWCNTs (shown in Fig. 7). Similar to suspended tubes, the substrate-supported tubes also show exponential dependence with voltage (figure 6a) and linear rise with time (figure 6c), but the effect is much less pronounced and shows delayed onset. Suspended tubes show increment in current around the TLP voltage of 4 V (figure 2a), while current through the substrate-supported tubes increases around 10 V (figure 6a). The reduction in effect is attributed to underlying substrate, which plays a vital role in cooling down the tube. Coupling between hot carriers in the nanotube and polar  $\text{SiO}_2$  substrate takes away a major fraction of heat to substrate [12]. Hot, energetic electrons in substrate supported nanotube dissipate their energy directly to phonon modes of the underlying polar substrate. Rate of transfer of energy through this process is more than that of energy transfer to optical phonons of the nanotube lattice, consequently former process dominates over the latter one and temperature of the nanotube does not rise in spite of conducting large amount of current through diffusive transport [13].

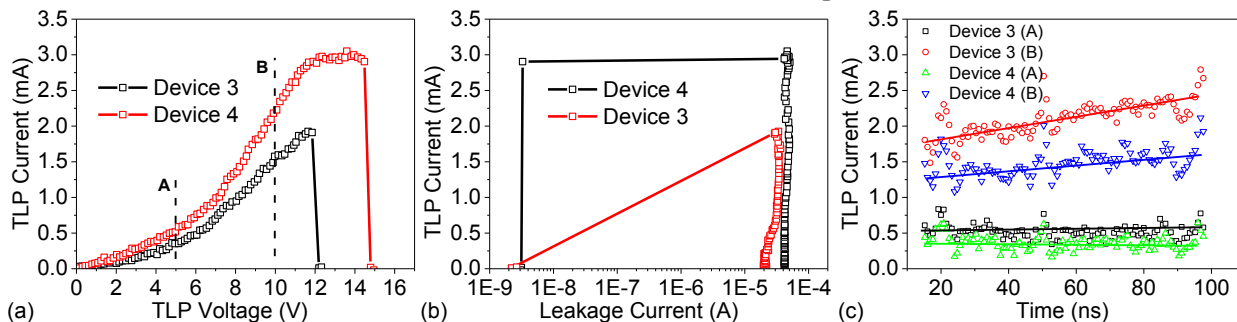


Figure 6: (a) TLP characteristics of substrate-supported tubes (b) change in low-bias DC current w.r.t. TLP current (c) Transient waveforms at two different TLP voltages marked in (a). Unlike suspended tubes, the transient rise in collapsed tubes is relatively less pronounced and happens at much higher voltage.

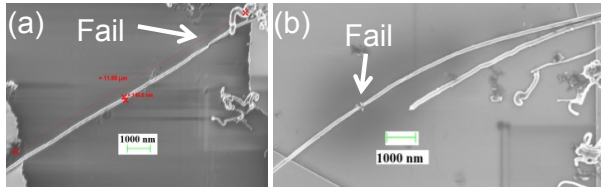


Figure 7: (a) SEM image of Device 3 (b) SEM image of Device 4. Both the devices are resting on  $\text{SiO}_2$ .

Since hot electrons get de-energize due to underlying polar substrate, compared to suspended tube, the temperature of hot contact in substrate-supported tube shows relatively less increment and happens at higher TLP voltage. Consequently, the substrate-supported tube shows relatively less rise in current. Moreover, since the cold contact does not heats-up significantly, therefore, Fermi-Dirac distribution does not smears-in higher sub-bands, which in-turn results in conduction through lower sub-bands only.

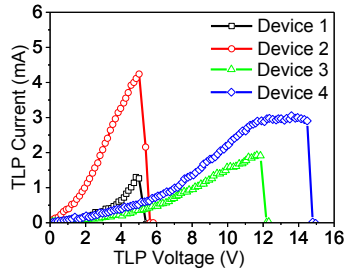


Figure 8: Comparison of TLP characteristics of suspended tubes (Device 1 and Device 2) with substrate supported tubes (Device 3 and Device 4). Compared to suspended tubes, the substrate supported tubes show higher breakdown voltage and carry relatively less amount of current.

Figure 8 compares the TLP characteristics of suspended MWCNTs with substrate supported MWCNTs and highlights the higher breakdown voltage, but relatively less current in case of substrate-supported CNTs. The reason behind this observation is attributed to interaction of energetic electrons with substrate, which results in - 1) transfer of heat to the substrate and increases the breakdown voltage as lattice heats-up at higher voltages 2) lower current compared to suspended tubes, because of de-energization of electrons along the length of the tube and conduction through lower-sub-bands only. Figure 8 also reveals that current density through these tubes is of the order of  $10 \text{ MA/cm}^2$  (average current = 1 mA, average diameter = 50 nm). Copper interconnects offer current density of the order of  $1 \text{ MA/cm}^2$  under steady state [14] and  $70 \text{ MA/cm}^2$  [15] during ESD stress. Present work reports similar ESD current for both MWCNT and copper interconnects, while previous work [6] has reported higher value for MWCNT interconnects. This is because current through MWCNTs depends on various process

parameters (diameter, number of shells, deposition technique, passivation, number of tubes etc.). Since, CNTs are resilient towards electro-migration and mean free path of scattering in CNTs is more than that in copper, improvements in the process technology can result in interconnects, which are expected to be better and robust than their copper counterparts.

Next we focus our attention to the effect of smaller TLP pulses (50 ns) on substrate-supported MWCNTs. Figure 9 shows the TLP characteristics of substrate supported tubes excited with 50 ns long pulses. The characteristics show breakdown voltage higher than that of the suspended tubes, while showing shell-by-shell breakdown. Unlike the other substrate-supported devices discussed previously (figure 6a), characteristics shown in figure 9a shows huge exponential increase after a particular threshold voltage. This dissimilarity from the previous case can be explained by simultaneous analysis of the device leakage and TLP characteristics. Note that before shell-by-shell breakdown, the devices show increase in leakage current with TLP current (figure 9b). Such an increase in leakage was not present in the substrate-supported devices discussed previously (figure 6b). We attribute this increase in leakage to current annealing of the interface between nanotube and metal contacts. Joule heating at high TLP currents strengthens the bond between  $d$ -orbital of metal and un-hybridized  $p$ -orbital of the outermost shell of the nanotube, which in turn results in increase in current. Note that unlike the increase in leakage current observed in devices 5 and 6 (figure 9b), the leakage currents reported previously (figure 2b and figure 6b) does not show any significant change with TLP current.

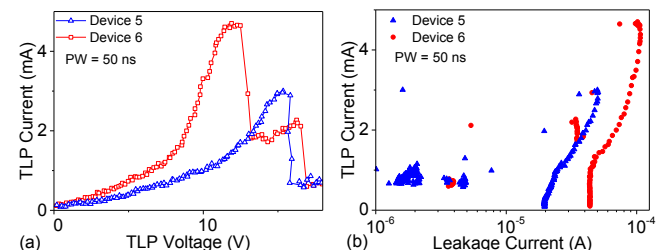


Figure 9: TLP characteristics of substrate-supported MWCNTs, excited by pulses of width 50 ns. Note that leakage current increases before showing shell-by-shell breakdown.

## V. Conduction through Inner Shells

Figure 10 shows ESD current conduction through inner shells of an MWCNT. Inner shells were made accessible through controlled shell-by-shell breakdown. This kind of ESD stress initiated breakdown is unique to MWCNTs and is discussed in

detail in [6]. Conduction before first breakdown and second breakdown shows linear rise in current with time, while the conduction after third breakdown shows relatively less increment with time.

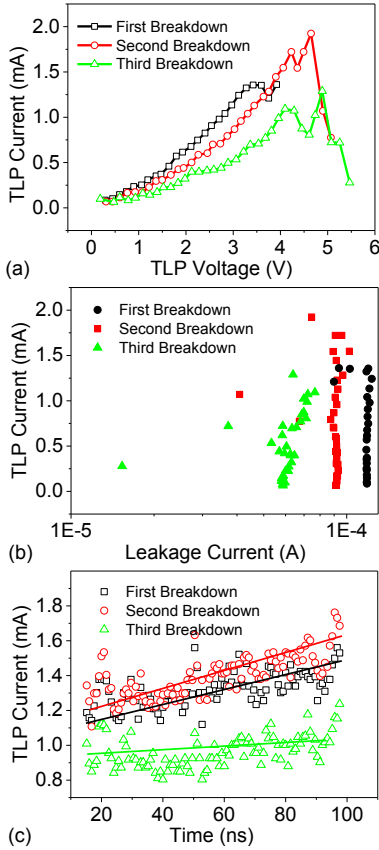


Figure 10: (a) ESD current through inner shells; (b) fall in current through nanotubes after a particular TLP current, indicates breakdown of few outer shells; (c) Change in ESD current with time. Note that current through outer shells (first and second breakdown) increases with time, while current through inner shells (third breakdown) remains constant with time. Transient data is shown for TLP voltage of 4 V.

High-bias conduction through a MWCNT takes place via tunneling across non-crossing sub-bands. Band-gap between these bands depends on diameter and is given by [11]

$$\Delta E_{NC} = 2t_0 \sin\left(\frac{\pi}{N}\right) \quad (3)$$

where,  $t_0$  is the hopping parameter between nearest neighbor carbon atoms and  $N$  decides the diameter of the tube. Consequently, the band-gap increases with subsequent breakdowns. Although, heat propagates from hot to cold contact for every shell, the number of conduction bands smeared by the Fermi distribution does not increase for thinner shells (figure 11). As a result, conduction of ESD current through thick shells

increases with time, but the conduction through thin shells remains relatively constant with time.

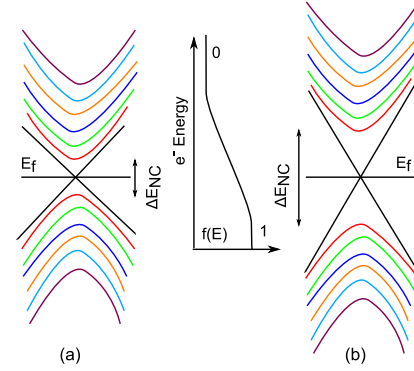


Figure 11: Sub-bands of (a) outer and (b) inner shells of a MWCNT. Note that the number of sub-bands smeared by Fermi-Dirac distribution decreases with decrease in diameter of the shell.

## VI. Effect of Length on ESD Current

Figure 12 shows the length dependence of thermal energy assisted rise in ESD current through MWCNTs. In all the cases, after a certain threshold voltage, current increases with time. The threshold voltage, in turn, increases with length, while the rise in current decreases with length. Overall effect is less pronounced for longer tubes. With increase in length, electrical transport through MWCNT turns from ballistic to diffusive. Less scattering in short ballistic tube paves the unimpeded rise in current with time. As a result, the upper limit of rise in current through such tubes is decided by the time taken to achieve thermal equilibrium and the sub-bands available for conduction. In diffusive tubes, scattering along the length impedes the flow of electrons and results in a reduction in transient rise in current. Consequently, the transient increase in current initially rises with voltage and then decreases after showing a peak, at which rise in current due to thermal energy gets nullified by reduction due to scattering.

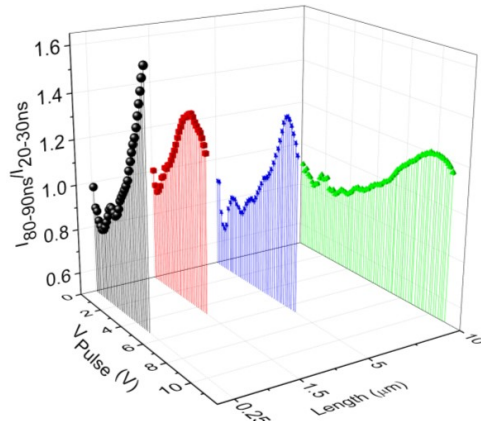


Figure 12: Change in relative increase in ESD current with pulse voltage and tube's length.

## VII. Conclusion

Through detailed TLP analysis, ESD current through MWCNTs was traced down to sub-bands of individual shells. It was revealed that thermal energy due to high ESD stress spreads-out current to higher sub-bands and results in an increase in the device current. In substrate-supported tubes, polar substrate takes away the thermal energy and results in relatively less ESD current, which flows only through a few lower energy sub-bands. The study shows that tubes encapsulated in polar materials like SiO<sub>2</sub> are best suited for ESD robust interconnects.

## Acknowledgement

Authors acknowledge the Department of Science and Technology, Govt. of India for financial support (project grant number: SB/S3/EECE/063/2014), Prof. Srinivasan Raghavan (CeNSE, IISc), Prof. K.K. Nanda (MRC, IISc) and Mr. Ravi Nandan (MRC, IISc) for their help in material synthesis and Dr. T.V. Prabhakar (DESE, IISc) for fruitful discussion and support on instrumentation. We also thank Dr. Nathan D Jack for mentoring the paper.

## References

- [1] N. Srivastava, R.V. Joshi, and K. Banerjee, "Carbon nanotube interconnects: implications for performance, power dissipation and thermal management". IEEE International Electron Devices Meeting, 2005
- [2] H. Li, W.Y. Yin, K. Banerjee, and J.F. Mao, "Circuit modeling and performance analysis of multi-walled carbon nanotube interconnects", IEEE Trans. on Electron Devices, , Vol. 55, 2008
- [3] A. Naeemi and J.D. Meindl, "Compact Physical Models for Multiwall Carbon-Nanotube Interconnects", IEEE Electron Device Letters, Vol. 27, 2006
- [4] A. Nieuwoudt and Y. Massoud, "On the Optimal Design, Performance, and Reliability of Future Carbon Nanotube-Based Interconnect Solutions", IEEE Trans. on Electron Devices, Vol. 55, 2008
- [5] G. F. Close and H. S. P. Wong, "Fabrication and Characterization of Carbon Nanotube Interconnects," IEEE International Electron Devices Meeting, 2007
- [6] M. Shrivastava and H. Gossner, "ESD Investigations of Multiwalled Carbon Nanotubes" IEEE TDMR, March 2013
- [7] M. Shrivastava and H. Gossner, "ESD behavior of metallic carbon nanotubes," Electrical Overstress/Electrostatic Discharge Symposium (EOS/ESD), 2014
- [8] A. Mishra and M. Shrivastava "New Insights on the ESD Behavior and Failure Mechanism of Multi Wall CNTs" to appear in IEEE IRPS 2016
- [9] J. Moscatello, V. Kayastha, B. Ulmen, A. Pandey, S.W., A. Singh, and Y.K. Yap, "Surfactant-free dielectrophoretic deposition of multi-walled carbon nanotubes with tunable deposition density", Carbon, Vol. 48, 2010
- [10] S. Datta, "Electronic Transport in Mesoscopic Systems", Cambridge University Press, 2011
- [11] M. P. Anantram, "Current-carrying capacity of carbon nanotubes", Phys. Rev. B, Vol. 62, 2000
- [12] K.H. Baloch, N. Voskanian, M. Bronsgeest and J. Cumings, "Remote Joule heating by a carbon nanotube", Nature Nanotechnology, Vol. 7, 2007

- [13] S.V. Rotkin, V Perebeinos, A.G. Petrov, and P Avouris, "An essential mechanism of heat dissipation in carbon nanotube electronics", Nano letters, Vol. 9, 2009
- [14] P.C. Wang and R.G. Filippi, "Electromigration threshold in copper interconnects". Applied Physics Letters, Vol. 78, 2001
- [15] K. Banerjee, A. Amerasekera and Chenming Hu, "Characterization of VLSI circuit interconnect heating and failure under ESD conditions," IEEE International Reliability Physics Symposium, 1996